Theory of twinning structures in the orthorhombic phase of ferroelectric perovskites

1997 J. Phys.: Condens. Matter 9 4467

(http://iopscience.iop.org/0953-8984/9/21/012)

J. Phys.: Condens. Matter **9** (1997) 4467–4482. Printed in the UK PII: S0953-8984(97)76998-4

Theory of twinning structures in the orthorhombic phase of ferroelectric perovskites

X R Huang, S S Jiang, X B Hu and W J Liu

National Laboratory of Solid State Microstructures and Department of Physics, Nanjing University, Nanjing 210093, People's Republic of China

Received 8 August 1996, in final form 9 December 1996

Abstract. The microstructures of coherent 180°, 90°, and 120° domain walls in the orthorhombic phase of ferroelectric perovskites have been studied on the basis of Landau–Ginzburg theory for the first-order phase transitions. It is found that for the space profile of the polarization within an uncharged wall layer, the normal component always remains zero or constant, while the component parallel to the wall plane has two kinds of inhomogeneous configuration, one of the 'Ising type' and the other of the 'Bloch type'. Quasi-one-dimensional analytic solutions for polarization components, elastic strains, and clamping stresses are obtained for the Ising-type 180°, 90°, and 120° wall interfaces. The structural characteristics and physical properties of the Bloch-type walls are also illustrated and discussed. All of the theoretical results are functions of macroscopic quantities for perovskite crystals, and can be applied to real systems when these quantities are obtained from experiments.

1. Introduction

Many ferroelectric perovskites, such as $BaTiO_3$ and the $KTa_{1-x}Nb_xO_3$ ($0.05 < x \leqslant 1$) series, exhibit the classical phase transition sequence from the paraelectric cubic phase to ferroelectric tetragonal, orthorhombic, and rhombohedral phases upon cooling [1–4]. A common phenomenon of the three ferroelectric phases is the twinning between energetically equivalent domains. Well known examples are the 180° and 90° twins in the tetragonal phase, whose domain morphology and dynamics have been investigated extensively [5–8]. In the orthorhombic phase, the polar axes of a pair of adjoining domains can take any two of the twelve equivalent ⟨110⟩ directions of the prototypic cubic lattice, which gives rise to four kinds of twinning structure defined as 180°, 90°, 120°, and 60° twins, respectively, depending on the size (in degrees) of the angle between the two polarization vectors. Generally, a domain wall (twin boundary) connecting two twinned domains contains excess energy compared to a single-domain structure, and this energy is minimized when the polarization vectors are arranged to satisfy $\nabla \cdot \boldsymbol{P} = 0$ within the wall layer. Most domain walls in ferroelectrics satisfy this condition, and are called 'uncharged walls' (charge-neutral walls) [9, 10]. According to this rule, an uncharged 180° wall in an orthorhombic perovskite is always parallel to the polar axes of the domains separated by the wall. Besides the charge neutrality condition, the orientations of uncharged 90°, 120°, and 60° walls also satisfy strain compatibility between the adjacent domains [11]. For this reason, the 90° and 120° walls are parallel to {100} and {110} lattice planes, respectively. The 60° walls determined by the charge neutrality and strain compatibility are along the $\{hkk\}$ lattice planes with $h/k = (e_a - e_c)/2e_t$ (e_a, e_c, and e_t are the strain components of the

0953-8984/97/214467+16$19.50

homogeneous orthorhombic lattice with respect to the cubic lattice; see section 2) [12]. In the rhombohedral phase, the polar axes are the eight ⟨111⟩ directions, and consequently 180°, 118°, and 62° twinnings are possible.

Although the theories of twinning rules for ferroic crystals have been well elaborated [13], an understanding of domain wall structure remains a most important issue in the study of ferroelectricity at present. In fact, the structure of domain walls plays an essential role in the ferroelectric behaviours of perovskite and other crystals: (i) the morphology of a domain is determined by the anisotropy of the wall energy; (ii) the switching of domains in external (electrical and mechanical) fields is actually realized by the wall motion, i.e. the nucleation and growth of new domains in the vicinity of the walls; (iii) domain walls are natural nucleation sites for ferroelectric phase transitions due to their special structure deviating from homogeneous domains; and (iv) the variation of domain wall energy with temperature governs domain evolution through the process of creation and annihilation of walls upon heating and cooling [2, 14–16]. However, since domain walls are usually a few lattice constants wide, it is difficult to observe and measure directly their microstructure, including the polarization profiles, energy, and inhomogeneous elastic strains. The only possible way is to model the wall structure on the basis of its relations with the macroscopic properties of the bulk crystal, and the Landau–Ginzburg (LG) theory provides phenomenologically a particularly useful method for this purpose. This theory takes into account the nonlinear and nonlocal characteristics of the polarization as well as the electromechanical coupling, from which quasi-one-dimensional (Q1D) kink solutions for the space profiles of the polarization components, the elastic strains, and the mechanical stresses of the walls can be deduced. In particular, the general properties of domain walls obtained from the LG theory, such as the wall broadening and wall energy variation, are verifiable by experiments [15–19].

Because 180°, 90°, 120°, and 60° walls can coexist in the orthorhombic phase of ferroelectric perovskites, the domain structures are more complicated than that in the tetragonal phase. Actually, the ferroelectric perovskites (e.g. $KNbO_3$) which are orthorhombic at room temperature are heavily twinned, and the complex domain patterns greatly affect the technological applications of the crystals [20]. In order to understand these twinning phenomena, we use the LG theory in this paper to present a full description of the 180°, 90°, and 120° wall structures which occur frequently in the orthorhombic phase. The theoretical models presented depend only on fifteen macroscopic parameters obtainable experimentally, and are applicable to the real system.

2. The model for the free energy

The ferroelectric phase transitions of most perovskites are of first order. For these transitions, the Helmholtz free-energy density of the homogeneous system

$$F(P_i, P_{i,j}, e_{kl}) = F_L(P_i) + F_{el}(e_{kl}) + F_c(P_i, e_{kl}) \tag{1}$$

is invariant under the $m3m$ symmetry of the cubic phase, and can be expanded in power series in the polarization $\{P_i\}$ and the elastic strain tensor $\{e_{kl}\}$ $(i, j, k, l = 1, 2, 3)$:

$$F_L = \alpha_1 \sum_i P_i^2 + \alpha_{11} \sum_i P_i^4 + \alpha_{12} \sum_{i<j} Pi^2 P_j^2 + \alpha_{111} \sum_i P_i^6 + \alpha_{112} \sum_{i\neq j} P_i^2 P_j^4 + \alpha_{123} P_1^2 P_2^2 P_3^2 \tag{2a}$$

$$F_{el} = \frac{c_{11}}{2} \sum_k e_{kk}^2 + c_{12} \sum_{k<l} e_{kk} e_{ll} + 2c_{44} \sum_{k<l} e_{kl}^2 \tag{2b}$$

$$F_c = -q_{11}\sum_i e_{ii}P_i^2 - \frac{q_{12}}{2}\sum_{i\neq j\neq k} e_{ii}(P_j^2 + P_k^2) - 2q_{44}\sum_{i<j} e_{ij}P_iP_j \tag{2c}$$

where the α_i, α_{ij}, α_{ijk} are the dielectric stiffness and high-order stiffness coefficients at *constant strain*, the c_{ij} are the second-order elastic constants at constant polarization, and the q_{ij} are the electrostrictive coefficients [16, 21]. In the absence of external force, i.e. where $\sigma_{ij} = \partial F/\partial e_{ij} = 0$ (the σ_{ij} are the components of the total Cauchy stress tensor), the relations between the polarization and strain components are

$$\begin{aligned} e_{ii} &= Q_{11}P_i^2 + Q_{12}(P_j^2 + P_k^2) \qquad &\text{for } i \neq j \neq k \\ e_{ij} &= \frac{1}{2}Q_{44}P_iP_j \qquad &\text{for } i \neq j \end{aligned} \tag{3}$$

with the definitions

$$\begin{aligned} Q_{11} &= \frac{q_{11}(c_{11}+c_{12}) - 2q_{12}c_{12}}{(c_{11}-c_{12})(c_{11}+2c_{12})} \\ Q_{12} &= \frac{q_{12}c_{11} - q_{11}c_{12}}{(c_{11}-c_{12})(c_{11}+2c_{12})} \\ Q_{44} &= \frac{q_{44}}{c_{44}}. \end{aligned} \tag{4}$$

By substituting equation (3) into equations (2*b*) and (2*c*), the total free-energy density F may be reexpressed so as to have the same form as F_L, except that the coefficients α_{11} and α_{12} in equation (2*a*) should be replaced by

$$\begin{aligned} \alpha'_{11} &= \alpha_{11} + \frac{-q_{11}^2(c_{11}+c_{12}) + 4q_{11}q_{12}c_{12} - 2q_{12}^2c_{11}}{2(c_{11}-c_{12})(c_{11}+2c_{12})} \\ \alpha'_{12} &= \alpha_{12} + \frac{q_{11}^2c_{12} - 2q_{11}q_{12}c_{11} + q_{12}^2(2c_{12}-c_{11})}{2(c_{11}-c_{12})(c_{11}+2c_{12})} - \frac{q_{44}^2}{2c_{44}}. \end{aligned} \tag{5}$$

In the orthorhombic phase, the spontaneous polarization has the form $\boldsymbol{P} = (P_0, P_0, 0)$, where P_0 is the greater root of the equation

$$\alpha_1 + (2\alpha'_{11} + \alpha'_{12})P^2 + 3(\alpha_{111} + \alpha_{112})P^4 = 0. \tag{6}$$

Compared with the case of the cubic lattice, the nonzero strain components of the orthorhombic lattice are

$$\begin{aligned} e_{11} &= e_{22} = (Q_{11} + Q_{12})P_0^2 = e_a \\ e_{33} &= 2Q_{12}P_0^2 = e_c \\ e_{12} &= Q_{44}P_0^2 = e_t. \end{aligned} \tag{7}$$

In an inhomogeneous system with a gradient distribution of the polarization, the free energy must contain the gradient energy whose density to the lowest order can be written as

$$F_G = \frac{g_{11}}{2}\sum_i P_{i,i}^2 + g_{12}\sum_{i<j} P_{i,i}P_{j,j} + \frac{g_{44}}{2}\sum_{i<j}(P_{i,j} + P_{j,i})^2 \tag{8}$$

for cubic symmetry. Here $P_{i,j}$ denotes the differential of P_i with respect to the position coordinates x_j [16]. In the following sections, we concentrate on the inhomogeneous orthorhombic phase containing 180°, 90°, and 120° domain walls.

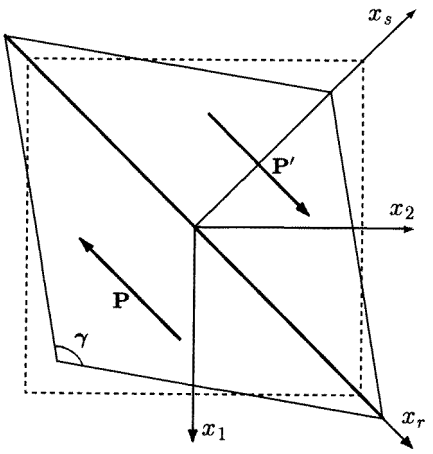

Figure 1. A schematic representation of a $(\bar{1}10)$ 180° twin in orthorhombic ferroelectric perovskites. The dashed lines indicate the prototypic cubic lattice. $\gamma = \pi/2 + 2e_t$, and the elastic strains are exaggerated.

3. The 180° wall

The 180° domain wall is an inhomogeneous transition layer connecting two domains with opposite polarization vectors. In this section, we consider the structure of a static $(\bar{1}10)$ 180° wall separating two domains with polarizations $(-P_0, -P_0, 0)$ and $(P_0, P_0, 0)$, respectively, as shown in figure 1. For convenience, the x_1x_2-plane is rotated along x_3 by 45° to make a new coordinate system $x_rx_sx_3$. Then the strain tensors $\{\eta_{ij}\}$ $(i, j = r, s, 3)$ in the $x_rx_sx_3$ system are expressed with respect to $\{e_{ij}\}$ as

$$\begin{aligned}
\eta_{rr} &= \frac{1}{2}(e_{11} + e_{22} + 2e_{12}) \\
\eta_{ss} &= \frac{1}{2}(e_{11} + e_{22} - 2e_{12}) \\
\eta_{33} &= e_{33} \\
\eta_{rs} &= \frac{1}{2}(e_{22} - e_{11}) \\
\eta_{r3} &= \frac{1}{\sqrt{2}}(e_{13} + e_{23}) \\
\eta_{s3} &= \frac{1}{\sqrt{2}}(e_{23} - e_{13}).
\end{aligned} \tag{9}$$

In general, the domain wall inside a bulk crystal has the quasi-one-dimensional (Q1D) structure along the wall normal. For the present case, the structure depends only on x_s (abbreviated as s):

$$\boldsymbol{P} = \boldsymbol{P}(s) \qquad \eta_{ij} = \eta_{ij}(s) \qquad \sigma_{ij} = \sigma_{ij}(s). \tag{10}$$

Under these conditions, the charge neutrality condition $\boldsymbol{\nabla} \cdot \boldsymbol{P} = 0$ becomes

$$P_s = 0 \qquad P_r = \sqrt{2}P_1 = \sqrt{2}P_2. \tag{11}$$

Thus, on defining the wall centre as $s = 0$, the boundary conditions of the 180° wall are

$$\lim_{s\to\pm\infty} P_r(s) = \pm\sqrt{2}P_0 \tag{12a}$$

$$\lim_{s\to\pm\infty} P_3(s) = 0 \tag{12b}$$

$$\lim_{s\to\pm\infty} \sigma_{ij}(s) = 0 \tag{12c}$$

$$\lim_{s\to\pm\infty} \{\eta_{ij}\} = \begin{pmatrix} e_a + e_t & 0 & 0 \\ & e_a - e_t & 0 \\ & & e_c \end{pmatrix}. \tag{12d}$$

In the absence of dislocation and inclination, the compatibility relations of the strain components [22], $\eta_{ii,jk} + \eta_{jk,ii} = \eta_{ij,ik} + \eta_{ik,ij}$ for $ijk = rss, r33, s33, rs3, sr3, 3rs$, yield

$$\eta_{33,ss} = 0 \qquad \eta_{rr,ss} = 0 \qquad \eta_{r3,ss} = 0. \tag{13}$$

Integrating equation (13) on the basis of the boundary condition of equation (12*d*) leads to

$$\eta_{33} \equiv e_c \qquad \eta_{r3} \equiv 0 \qquad \eta_{rr} \equiv e_a + e_t. \tag{14}$$

Then in view of equations (14) and (9), F_{el} and F_c can be rewritten as

$$\begin{aligned} F_{el} &= \frac{\hat{c}_+}{4}\eta_{ss}^2 + \left[\frac{\hat{c}_-}{2}(e_a + e_t) + c_{12}e_c\right]\eta_{ss} + (c_{11} - c_{12})\eta_{rs}^2 + 2c_{44}\eta_{s3}^2 \\ F_c &= -\frac{\hat{q}_-}{2}P_r^2\eta_{ss} - q_{12}P_3^2\eta_{ss} - \frac{\hat{q}_+(e_a + e_t) + 2q_{12}e_c}{2}P_r^2 - \left[q_{11}e_c + q_{12}(e_a + e_t)\right]P_3^2 \end{aligned} \tag{15}$$

where $\hat{c}_\pm = c_{11} + c_{12} \pm 2c_{44}$ and $\hat{q}_\pm = q_{11} + q_{12} \pm q_{44}$. Since the wall is treated as an elastic solid here, it has the differential equation at equilibrium [22]

$$\sum_j \sigma_{ij,j} = 0 \qquad \text{for } i, j = r, s, 3. \tag{16}$$

From equations (10) and (12*c*), it follows immediately that

$$\sigma_{ij} = \frac{\partial(F_{el} + F_c)}{\partial\eta_{ij}} = 0 \qquad \text{for } ij = ss, rs, s3. \tag{17}$$

Substituting equation (15) into equation (17), one has

$$\begin{aligned} \eta_{ss} &= A + BP_r^2 + CP_3^2 \\ \eta_{rs} &= \eta_{s3} \equiv 0 \end{aligned} \tag{18}$$

where

$$\begin{aligned} A &= -\frac{\hat{c}_-(e_a + e_t) + 2c_{12}e_c}{\hat{c}_+} \\ B &= \frac{\hat{q}_-}{\hat{c}_+} \qquad C = \frac{2q_{12}}{\hat{c}_+}. \end{aligned} \tag{19}$$

Therefore, the combination of equations (2*a*), (8), (11), (15), and (18) gives the total free-energy density F as

$$\begin{aligned} F = {} & D_1P_r^2 + D_2P_3^2 + D_3P_r^4 + D_4P_3^4 + D_5P_r^2P_3^2 + D_6P_r^6 + D_7P_3^6 \\ & + D_8P_r^4P_3^2 + D_9P_r^2P_3^4 + \frac{g_{rs}}{2}P_{r,s}^2 + \frac{g_{44}}{2}P_{3,s}^2 \end{aligned} \tag{20}$$

with

$$
\begin{aligned}
&D_1 = \alpha_1 - \frac{\hat{q}_-}{2}A - \frac{\hat{q}_+}{2}(e_a + e_t) - q_{12}e_c \\
&D_2 = \alpha_1 - q_{12}(A + e_c) - q_{11}e_c \\
&D_3 = \frac{2\alpha_{11} + \alpha_{12}}{4} - \frac{\hat{q}_-}{4}B \qquad D_4 = \alpha_{11} - \frac{3}{2}q_{12}C \\
&D_5 = \alpha_{12} - q_{12}B \qquad D_6 = \frac{\alpha_{111} + \alpha_{112}}{4} \\
&D_7 = \alpha_{111} \qquad D_8 = \frac{2\alpha_{112} + \alpha_{123}}{4} \qquad D_9 = \alpha_{112}
\end{aligned}
\tag{21}
$$

and

$$
g_{rs} = \frac{g_{11} - g_{12}}{2}. \tag{22}
$$

It should be noted that the constant terms in equations (15) and (20) have been neglected since they do not influence the following results. By inserting equation (20) into the Euler equations [16, 23]

$$
\sum_j \frac{\partial}{\partial x_j}\frac{\partial F}{\partial P_{i,j}} - \frac{\partial F}{\partial P_i} = 0 \qquad \text{for } i, j = r, s, 3 \tag{23}
$$

one obtains the static equilibrium conditions of the 180° wall:

$$
g_{rs}P_{r,ss} = 2D_1P_r + 4D_3P_r^3 + 2D_5P_rP_3^2 + 6D_6P_r^5 + 4D_8P_r^3P_3^2 + 2D_9P_rP_3^4 \tag{24a}
$$

$$
g_{44}P_{3,ss} = 2D_2P_3 + 4D_4P_3^3 + 2D_5P_r^2P_3 + 6D_7P_3^5 + 2D_8P_r^4P_3 + 4D_9P_r^2P_3^3. \tag{24b}
$$

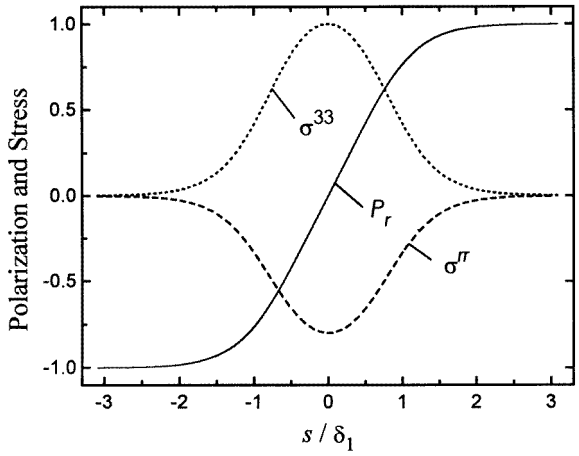

Figure 2. Space profiles of the polarization and clamping stress components scaled in dimensionless forms for the Ising-type 180° wall structure.

It is apparent that equations (24*a*) and (24*b*) have the analytic kink solution which satisfies the boundary conditions equations (12*a*) and (12*b*):

$$
P_r(s) = \sqrt{2}P_0\frac{\sinh(s/\delta_1)}{\sqrt{q_1^2 + \cosh^2(s/\delta_1)}} \qquad P_3(s) \equiv 0 \tag{25}
$$

where

$$q_1^2 = \frac{2P_0^2}{4P_0^2 - D_3/D_6}$$
$$\delta_1 = \frac{1}{2P_0}\sqrt{\frac{g_{rs}}{6D_6P_0^2 - D_3}}. \tag{26}$$

Here δ_1 is conventionally used to characterize half the width of the 180° wall. The space profile of the polarization represented by the solution of equation (25) is illustrated in figure 2. For this wall, the only position-dependent strain component is $\eta_{ss}(s) = A + BP_r^2(s)$, and the nonvanishing stress components required to sustain the Q1D structure are

$$\sigma_{33} = (c_{12}B - q_{12})\left[P_r^2(s) - 2P_0^2\right]$$
$$\sigma_{rr} = \left(\frac{c_{11} + c_{12}}{2}B - \frac{q_{11} + q_{12}}{2}\right)\left[P_r^2(s) - 2P_0^2\right]. \tag{27}$$

Since the decrease of $|P_r|$ within the wall layer tends to induce shrinkage and expansion in the dimensions along x_r and x_3, respectively, the two stresses required to resist this tendency have opposite signs: $\sigma_{rr} \leqslant 0$ and $\sigma_{33} \geqslant 0$, as presented schematically in figure 2. According to equation (3), removal of these stresses may, in principle, lead to 'misfit dislocations' in the wall region for bulk crystals (although it may be different for thin films). Therefore, a coherent 180° wall in a bulk crystal is always constrained. In particular, when no external force is applied on the wall, the two normal stresses in equation (27) can be provided automatically by the two domains (the domain-clamping effect).

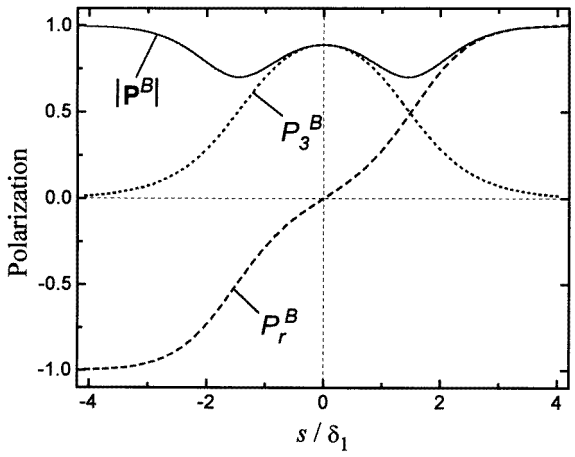

Figure 3. Polarization profiles of the Bloch-type 180° wall structure. The curves have been obtained by numerical integration of equations (24*a*) and (24*b*) with the same input parameters as were used for calculating the curves in figure 2. Note that not only does the magnitude of the polarization change, but also a rotation of $\boldsymbol{P}^B$ occurs. The width of the Bloch-type wall is generally greater than that of the Ising-type wall.

The solution given as equation (25) indicates that the polarization vector $\boldsymbol{P} = [P_r(s), 0, 0]$ is always parallel to the x_r-axis across the wall. Such a wall is often called an 'Ising-type' wall [24]. However, the solutions of equations (24*a*) and (24*b*) are not unique in general. It can be proved that, besides the kink solution, there may exist another solution which contains two variable polarization components $P_r(s)$ and $P_3(s)$ ($\neq 0$) within

the wall layer. This kind of wall structure is of 'Bloch type', and in this paper its solutions are denoted by the superscript 'B'. In order to obtain numerically $P_r^B(s)$ and $P_3^B(s)$, it is necessary to integrate equations (24*a*) and (24*b*) from the wall centre $s = 0$ to $\pm\infty$. According to equations (12*a*) and (12*b*), one may naturally assume that $P_r^B(0) = 0$ and $P_{3,s}^B(0) = 0$. The other two initial values $P_3^B(0)$ and $P_{r,s}^B(0)$ are related to each other by the first integrals of equations (24*a*) and (24*b*)

$$\frac{g_{rs}}{2}P_{r,s}^2 + \frac{g_{44}}{2}P_{3,s}^2 = D_1P_r^2 + D_2P_3^2 + D_3P_r^4 + D_4P_3^4 + D_5P_r^2P_3^2 + D_6P_r^6 + D_7P_3^6 + D_8P_r^4P_2^2 + D_9P_r^2P_3^4 - F_0 \tag{28}$$

where $F_0 = 2D_1P_0^2 + 4D_3P_0^4 + 8D_6P_0^6$ corresponds to the free-energy density of the homogeneous state. Therefore, by scanning either $P_3(0)$ or $P_{r,s}(0)$ during the integration, one can obtain the solution $[P_r^B(s), P_3^B(s)]$ which satisfies the boundary conditions of equations (12*a*) and (12*b*) [25]. The profiles of P_r^B, P_3^B, and $|\boldsymbol{P}^B|$ calculated with the same input parameters as for figure 2 are plotted in figure 3, in which the total polarization $\boldsymbol{P}^B$ is *rotated* from $(0, -\sqrt{2}P_0, 0)$ to $(0, \sqrt{2}P_0, 0)$ across the Bloch-type wall, though the magnitude of $\boldsymbol{P}^B$ varies with x_s. Like the Ising-type wall, the Bloch-type wall has no shear deformation, and only η_{ss}^B, which is related to P_r^B and P_3^B by equation (18), varies along the x_s-axis. The stresses required to sustain such a wall are σ_{rr}^B, σ_{33}^B, and σ_{r3}^B, and they are functions of P_r^B and P_3^B. In fact, the coexistence of P_r^B and P_3^B within the wall layer tends to produce a shear deformation within the wall plane, but this tendency is resisted by the shear stress σ_{rs}^B.

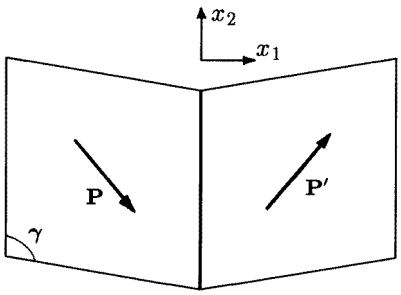

Figure 4. The arrangement of a twinned 'V-shaped' crystal in orthorhombic ferroelectric perovskites. The twin boundary is a (100) 90° wall.

4. The 90° wall

The 90° wall of ferroelectric perovskites connects two domains whose polarization vectors are nearly perpendicular to each other. The 90° domain walls in the tetragonal phase are along {110} lattice planes, but in the orthorhombic phase, they are parallel to the {100} planes. A (100) 90° wall separating two domains with polarization $(P_0, -P_0, 0)$ and $(P_0, P_0, 0)$, respectively, is shown in figure 4. For the Q1D structure of the wall, the space profile of the polarization only depends on the space variable x_1. In this case $\nabla \cdot \boldsymbol{P} = 0$ yields $P_1 \equiv P_0$. Then the boundary conditions are

$$\lim_{x_1 \to \pm\infty} P_3(x_1) = 0 \qquad \lim_{x_1 \to \pm\infty} P_2(x_1) = \pm P_0. \tag{29}$$

Similarly to the case for the 180° wall, the strain compatibility of the 90° wall requires three constant strain components in space:

$$e_{22} \equiv e_a \qquad e_{33} \equiv e_c \qquad e_{23} \equiv 0. \tag{30}$$

Consequently, the elastic energy of equation (2*b*) and the coupling energy of equation (2*c*) are rewritten as

$$F_{el} = \frac{c_{11}}{2} e_{11}^2 + c_{12}(e_a + e_c)e_{11} + 2c_{44}(e_{12}^2 + e_{13}^2) \tag{31a}$$

and

$$F_c = -q_{11}(e_{11}P_0^2 + e_a P_2^2 + e_c P_3^2) - q_{12}\left[e_a P_3^2 + e_c P_2^2 + e_{11}(P_2^2 + P_3^2)\right] - 2q_{44}P_0(e_{12}P_2 + e_{13}P_3). \tag{31b}$$

In figure 4, the equilibrium conditions of the stress tensor for the wall are $\sum_j \sigma_{ij,j} = 0$ ($i, j = 1, 2, 3$), which lead to $\sigma_{11} = \sigma_{12} = \sigma_{13} = 0$, or

$$\begin{aligned} e_{11} &= \frac{1}{c_{11}}\left[-c_{12}(e_a + e_t) + q_{11}P_0^2 + q_{12}(P_2^2 + P_3^2)\right] = A_1 + B_1(P_2^2 + P_3^2) \\ e_{12} &= \frac{q_{44}}{2c_{44}} P_0 P_2 = C_1 P_2 \qquad e_{13} = C_1 P_3. \end{aligned} \tag{32}$$

Substituting equation (32) into equation (31) and inserting $\boldsymbol{P} = (P_0, P_2, P_3)$ into equation (2*a*), one can write the total free-energy density of the 90° wall as

$$F = \frac{g_{44}}{2}(P_{2,1}^2 + P_{3,1}^2) + E_1 P_2^2 + E_2 P_3^2 + E_3(P_2^4 + P_2^4) + E_4 P_2^2 P_3^2 + \alpha_{111}(P_2^6 + P_3^6) + \alpha_{112} P_2^2 P_3^2 (P_2^2 + P_3^2) \tag{33}$$

where the constants E_i are defined as

$$\begin{aligned} E_1 &= \alpha_1 + \alpha_{12}P_0^2 + \alpha_{112}P_0^4 - 2c_{44}C_1^2 - q_{11}e_a - q_{12}(e_a + A_1) \\ E_2 &= E_1 + (q_{11} - q_{12})(e_a - e_c) \\ E_3 &= \alpha_{11} + \alpha_{112}P_0^2 - \frac{1}{2}q_{12}B_1 \\ E_4 &= \alpha_{12} + \alpha_{123}P_0^2 - q_{12}B_1. \end{aligned} \tag{34}$$

The Euler equations given as equation (23) now become

$$g_{44}P_{2,11} = 2E_1P_2 + 4E_3P_2^3 + 2E_4P_2P_3^2 + 6\alpha_{111}P_2^5 + 4\alpha_{112}P_2^3P_3^2 + 2\alpha_{112}P_2P_3^4 \tag{35a}$$

$$g_{44}P_{3,11} = 2E_2P_3 + 4E_3P_3^3 + 2E_4P_2^2P_3 + 6\alpha_{111}P_3^5 + 2\alpha_{112}P_2^4P_3 + 4\alpha_{112}P_2^2P_3^3. \tag{35b}$$

Again, equations (35*a*) and (35*b*) have the kink solution

$$P_2(x_1) = P_0\frac{\sinh(x_1/\delta_2)}{\sqrt{q_2^2 + \cosh(x_1/\delta_2)}} \qquad P_3(x_1) \equiv 0 \tag{36}$$

where

$$\begin{aligned} q_2^2 &= \frac{P_0^2}{2P_0^2 - E_3/\alpha_{111}} \\ \delta_2 &= \frac{1}{P_0}\sqrt{\frac{g_{44}}{6\alpha_{111}P_0^2 - 2E_3}}. \end{aligned} \tag{37}$$

For this solution, it can be seen from equation (32) that $e_{13} = 0$, and the only two inhomogeneous strain components are $e_{11}(x_1) = A_1 + B_1P_3^2(x_1)$ and $e_{12} = C_1P_2(x_1)$.

The continuous variation of e_{12} from $-e_t$ to e_t indicates that the V-shaped bicrystal plotted in figure 4 is actually rounded at the wall centre, like to the ferroelastic domain wall in NdP_5O_{14} [18]. The associated nonzero stress components required to support the Q1D structure of the wall are given by

$$\begin{aligned}\sigma_{22}(x_1) &= (c_{12}B_1 - q_{11} - q_{12})\left[P_2^2(x_1) - P_0^2\right] \\ \sigma_{33}(x_1) &= (c_{12}B_1 - q_{12})\left[P_2^2(x_1) - P_0^2\right].\end{aligned} \tag{38}$$

Because the constants Q_{11} and Q_{12} defined in equation (7) are positive and negative, respectively for most perovskite ferroelectrics; the decrease of $|P_2(x_1)|$ from P_0 to zero upon approaching $x_1 = 0$ has a tendency to produce shrinkage and expansion of the wall lattice along x_2 and x_3 respectively. Therefore, the two normal stresses σ_{22} and σ_{33} required to keep e_{22} and e_{33} constant across the wall have opposite signs: $\sigma_{22} > 0$ and $\sigma_{33} < 0$. Moreover, it can be seen that the shape of the bicrystal divided by the 90° wall is rounded automatically in the x_1x_2-plane without any shear stress being applied.

The above solution for the 90° wall shows that the polarization has the form $\boldsymbol{P} = [P_0, P_2(x_1), 0]$. This kind of wall can still be considered as an Ising-type wall. Since equations (35*a*) and (35*b*) have the same forms as equations (24*a*) and (24*b*), they may also have the Bloch-type solution $\boldsymbol{P}^B = [P_0, P_2^B(x_1), P_3^B(x_1)]$, where $P_2^B(x_1)$ and $P_3^B(x_1)$ are nonzero within the wall layer. For the latter polarization configuration, the inhomogeneous strain components are e_{11}^B, e_{22}^B, and e_{13}^B (see equation (32)), and the stresses required to sustain the wall are σ_{22}^B, σ_{33}^B, and σ_{23}^B.

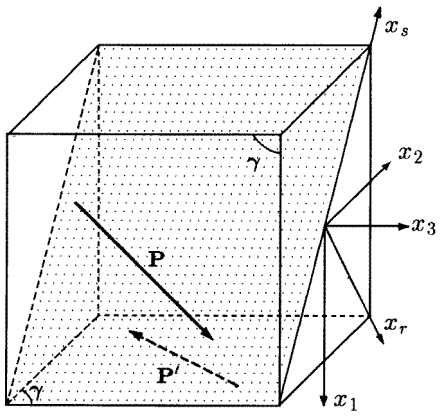

Figure 5. A schematic representation of a 120° twin in orthorhombic perovskites. The shaded interface indicates the uncharged wall. In the $x_1x_2x_3$ coordinate system, $\boldsymbol{P} = (P_0, 0, P_0)$ and $\boldsymbol{P}' = (0, P_0, -P_0)$.

5. The 120° wall

The strain compatibility of different orientation domains gives two kinds of planar wall called 'W walls' [13] in the orthorhombic phase of perovskite ferroelectrics: one is the 90° wall, and the other is the 120° wall which is strictly parallel to the {110} lattice planes (the electrically uncharged wall). The configuration of a (110) 120° wall is shown in figure 5, in which the $x_rx_sx_3$ coordinate system is generated by rotating the $x_1x_2x_3$ system along

x_3 by 45°. For the Q1D wall structure which varies only along x_r (abbreviated as r), the boundary conditions expressed in the $x_1x_2x_3$ coordinate system are

$$\lim_{r\to-\infty} \boldsymbol{P} = (P_0, 0, P_0) \qquad \lim_{r\to\infty} \boldsymbol{P} = (0, P_0, -P_0) \tag{39a}$$

and

$$\lim_{r\to-\infty} \{e_{ij}\} = \begin{pmatrix} e_a & 0 & e_t \\ & e_c & 0 \\ & & e_a \end{pmatrix} \qquad \lim_{r\to\infty} \{e_{ij}\} = \begin{pmatrix} e_c & 0 & 0 \\ & e_a & -e_t \\ & & e_a \end{pmatrix}. \tag{39b}$$

In the $x_rx_sx_3$ coordinate system, the polarization components P_r and P_s are expressed in terms of P_1 and P_2 as

$$P_r = (P_1 + P_2)/\sqrt{2} \qquad P_s = (P_2 - P_1)/\sqrt{2} \tag{40}$$

and the strain components η_{ij} are given by equation (9). The charge-neutral condition of the 120° wall, $\boldsymbol{\nabla}\cdot\boldsymbol{P} = 0$, now becomes $P_r \equiv P_0/\sqrt{2}$, and the boundary conditions for P_r and P_s are

$$\lim_{r\to\pm\infty} P_s = \pm P_0/\sqrt{2} \qquad \lim_{r\to\pm\infty} P_3 = \mp P_0. \tag{41}$$

The strain compatibility relations require three constant strain components, η_{ss}, η_{33}, and η_{s3}, across the wall. Then from equations (9) and (39*b*) it follows that

$$\eta_{ss} \equiv (e_a + e_c)/2 \qquad \eta_{33} \equiv e_a \qquad \eta_{s3} \equiv -e_t/\sqrt{2}. \tag{42}$$

The other three strain components are position dependent, and their boundary conditions are

$$\begin{aligned} &\lim_{r\to\pm\infty} \eta_{r3} = \mp e_t/\sqrt{2} \\ &\lim_{r\to\pm\infty} \eta_{rs} = \pm(e_a - e_c)/2 \\ &\lim_{r\to\pm\infty} \eta_{rr} = (e_a + e_c)/2. \end{aligned} \tag{43}$$

Inserting equation (42) into equation (9) and then inserting equation (9) into equations (2*b*) and (2*c*), one has

$$F_{el} = \frac{\hat{c}_+}{4}\eta_{rr}^2 + \frac{\hat{c}_-(e_a + e_c) + 4c_{12}e_a}{4}\eta_{rr} + (c_{11} - c_{12})\eta_{rs}^2 + 2c_{44}\eta_{r3}^2 \tag{44a}$$

$$\begin{aligned} F_c = &-\left(\frac{\hat{q}_+}{4}P_0^2 + \frac{\hat{q}_-}{2}P_s^2 + q_{12}P_3^2\right)\eta_{rr} - \sqrt{2}q_{44}P_0P_3\eta_{r3} - \sqrt{2}(q_{11} - q_{12})P_0P_s\eta_{rs} \\ &- \frac{\hat{q}_+(e_a + e_c)}{2}P_s^2 - \frac{q_{12}(e_a + e_c)}{2}P_3^2 - q_{11}e_aP_3^2 - q_{12}e_aP_s^2 + \sqrt{2}q_{44}e_tP_sP_3. \end{aligned} \tag{44b}$$

The three zero-stress components derived from equation (16) are now σ_{rr}, σ_{rs}, and σ_{r3}. By differentiating $F_{el} + F_c$ in equation (44) with respect to η_{rr}, η_{rs}, and η_{r3}, one obtains the three position-dependent strain components

$$\begin{aligned} \eta_{rr} &= A_2 + B_2P_s^2 + C_2P_3^2 \\ \eta_{rs} &= B_3P_s \\ \eta_{r3} &= C_3P_3 \end{aligned} \tag{45}$$

where

$$A_3 = \frac{\hat{q}_+ P_0^2 - \hat{c}_-(e_a + e_c) - 4c_{12}e_a}{2\hat{c}_+}$$
$$B_2 = \frac{\hat{q}_-}{\hat{c}_+} \qquad C_2 = \frac{2q_{12}}{\hat{c}_+} \tag{46}$$
$$B_3 = \frac{q_{11} - q_{12}}{\sqrt{2}(c_{11} - c_{12})} P_0 \qquad C_3 = \frac{q_{44}}{2\sqrt{2}c_{44}} P_0.$$

Substituting equation (45) into equation (44) and taking into account equations (2*a*) and (40), one can eventually write the total free-energy density as

$$F = G_1 P_s^2 + G_2 P_3^2 + \sqrt{2} q_{44} e_t P_s P_3 + G_4 P_s^4 + G_5 P_3^4 + G_6 P_s^2 P_3^2 + \frac{\alpha_{111} + \alpha_{112}}{4} P_s^6$$
$$+ \alpha_{111} P_3^6 + \frac{2\alpha_{112} + \alpha_{123}}{4} P_s^4 P_3^2 + \alpha_{112} P_s^2 P_3^4 + \frac{g_{rs}}{2} P_{s,r}^2 + \frac{g_{44}}{2} P_{3,r}^2 \tag{47}$$

where

$$G_1 = \alpha_1 + \frac{6\alpha_{11} - \alpha_{12}}{4} P_0^2 + \frac{15\alpha_{111} - \alpha_{112}}{16} P_0^4$$
$$- \frac{\hat{q}_-}{2} A_2 - (c_{11} - c_{12}) B_3^2 - \frac{\hat{q}_+}{4}(e_a + e_c) - q_{12} e_a \tag{48a}$$
$$G_2 = \alpha_1 + \frac{\alpha_{12}}{2} P_0^2 + \frac{2\alpha_{112} + \alpha_{123}}{16} P_0^4 - 2c_{44} C_3^2 - \frac{q_{12}}{2}(e_a + e_c) - q_{11} e_a - q_{12} A_2 \tag{48b}$$
$$G_4 = \frac{2\alpha_{11} + \alpha_{12}}{4} + \frac{15\alpha_{111} - \alpha_{112}}{8} P_0^2 - \frac{\hat{q}_-}{4} B_2 \tag{48c}$$
$$G_5 = \alpha_{11} + \frac{\alpha_{112}}{2} P_0^2 - \frac{q_{12}}{2} C_2 \tag{48d}$$
$$G_6 = \alpha_{12} + \frac{3\alpha_{112}}{2} P_0^2 - \frac{\alpha_{123}}{4} P_0^2 - \frac{\hat{q}_-}{2} C_2. \tag{48e}$$

It can be proved that the equilibrium equations for the 120° wall, obtained by inserting equation (47) into equation (23), have similar forms to equation (24) and equation (35). Like the 90° and 180° walls, the 120° wall also has two kinds of polarization configuration: one is of Ising type and the other of Bloch type. Here we only give the Ising-type solution.

In figure 4, it is the polarization vector $\boldsymbol{P}_\parallel = P_s \hat{\boldsymbol{s}} + P_3 \hat{\boldsymbol{k}}$ (parallel to the wall plane) that varies from $-(P_0/\sqrt{2})\hat{\boldsymbol{s}} + P_0 \hat{\boldsymbol{k}}$ to $(P_0/\sqrt{2})\hat{\boldsymbol{s}} - P_0 \hat{\boldsymbol{k}}$, where $\hat{\boldsymbol{s}}$ and $\hat{\boldsymbol{k}}$ are unit vectors along x_s and x_3, respectively. For the Ising type wall, the direction of $\boldsymbol{P}_\parallel$ is always parallel to $(1/\sqrt{2})\hat{\boldsymbol{s}} - \hat{\boldsymbol{k}}$, which means that

$$P_s \equiv -P_3/\sqrt{2}. \tag{49}$$

Then the total free-energy density in equation (47) becomes

$$F = H_1 P_3^2 + H_2 P_3^4 + H_3 P_3^6 + \frac{g_{rs} + 2g_{44}}{4} P_{3,r}^2 \tag{50}$$

where the H_i are defined as

$$H_1 = \frac{G_1}{2} + G_2 - q_{44} e_t$$
$$H_2 = \frac{G_4}{4} + G_5 + \frac{G_6}{2} \tag{51}$$
$$H_3 = \frac{33\alpha_{111} + 21\alpha_{112} + 2\alpha_{123}}{32}$$

and g_{rs} is defined by equation (22). In this case, the Euler equations reduce to

$$\frac{g_{rs}+2g_{44}}{2}P_{3,rr}=2H_1P_3+4H_2P_3^3+6H_3P_3^5 \tag{52}$$

in the $x_rx_sx_3$ coordinate system. Subsequently, the kink solutions for P_s and P_3 are

$$P_3(r)=-\frac{P_s(r)}{\sqrt{2}}=P_0\frac{\sinh(r/\delta_3)}{\sqrt{q_3^2+\cosh(r/\delta_3)}} \tag{53}$$

where

$$\begin{aligned} q_3^2&=\frac{P_0^2}{2P_0^2-H_2/3H_3}\\ \delta_3&=\frac{1}{2P_0}\sqrt{\frac{g_{rs}+2g_{44}}{3P_0H_3-H_2}}. \end{aligned} \tag{54}$$

On the basis of the above polarization profiles, the x_r-dependent strain components $\eta_{rr}(r)$, $\eta_{rs}(r)$, and $\eta_{r3}(r)$ can be quantified from equation (45). Furthermore, the stresses required to sustain the Q1D structure of the 120° wall are

$$\begin{aligned} \sigma_{ss}(r)&=\left(\frac{\hat{c}_-}{4}B_2\frac{\hat{q}_+}{4}-\frac{\hat{c}_-}{2}C_2-q_{12}\right)\left[P_3^2(r)-P_0^2\right]\\ \sigma_{s3}(r)&=\sqrt{2}q_{44}\left[P_3^2(r)-P_0^2\right]\\ \sigma_{33}(r)&=\left(\frac{c_{12}}{2}B_2+c_{12}C_2-q_{11}-\frac{q_{12}}{2}\right)\left[P_3^2(r)-P_0^2\right]. \end{aligned} \tag{55}$$

Here the normal stresses σ_{ss} and σ_{33} are present to resist the contraction and expansion of the wall in the lateral directions x_s and x_3, respectively. Compared with the Ising-type 180° and 90° walls, the Ising-type 120° wall has an extra stress component σ_{s3}. This stress is required to keep the shear strain η_{s3} constant across the wall (removal of σ_{s3} may induce interface disclinations). For a perfect crystal with free boundary conditions, the shear stress σ_{s3} is usually provided by the surface tension of the crystal while the normal stresses are due to the internal elastic force.

6. Discussion and conclusions

On the basis on the LG theory, we have developed continuum models of the 180°, 90°, and 120° domain wall structures in the orthorhombic phase of ferroelectric perovskites by taking into account the elastic interactions and the gradient energy induced by the polarization inhomogeneities. The models show that for an uncharged wall, the polarization component normal to the wall interface always keeps constant across the transition layer, while the component parallel to the wall has either an Ising-type profile or a Bloch-type profile. Due to the strain–polarization interactions, the elastic strains within the wall layer are also inhomogeneous, but the coherent wall keeps the lateral strains constant and permits no variation of the shear deformation in the planes parallel to the wall interface. Such a constrained state is sustained by position-dependent stresses.

In the framework of the LG theory, the solutions for 180°, 90°, and 120° walls obtained from the preceding processes are exact, and describe fully the three-dimensional configurations of the polarization, elastic strains, and clamping stresses. In particular, the solutions depend only on the fifteen coefficients of the expansion series of equations (2)

and (8). All of these coefficients correspond to certain macroscopic physical quantities of perovskite ferroelectrics. In general, the elastic Gibbs free energy

$$G = F - \sum_{ij} \sigma_{ij} e_{ij} \tag{56}$$

is used to correlate the dielectric, piezoelectric, and elastic properties of the paraelectric and ferroelectric phases. For single-domain perovskites, G may be expressed as

$$\begin{aligned} G = {} & \alpha_1^\sigma \sum_i P_i^2 + \alpha_{11}^\sigma \sum_i P_i^4 + \alpha_{12}^\sigma \sum_{i<j} Pi^2 P_j^2 + \alpha_{111}^\sigma \sum_i P_i^6 + \alpha_{112}^\sigma \sum_{i\neq j} P_i^2 P_j^4 \\ & + \alpha_{123}^\sigma P_1^2 P_2^2 P_3^2 - \frac{s_{11}^P}{2} \sum_i \sigma_{ii}^2 - s_{12}^P \sum_{i<j} e_{ii} e_{jj} - \frac{s_{44}^P}{2} \sum_{i<j} e_{ij}^2 \\ & - Q_{11} \sum_i \sigma_{ii} P_i^2 - \frac{Q_{12}}{2} \sum_{i\neq j\neq k} \sigma_{ii} (P_j^2 + P_k^2) - Q_{44} \sum_{i<j} \sigma_{ij} P_i P_j \end{aligned} \tag{57}$$

where the α_1^σ, α_i^σ, α_{ijk}^σ are the dielectric stiffness and high-order stiffness coefficients measured at *constant stress* (different from the α_1, α_{ij}, and α_{ijk} of the clamped state; see equation (2*a*)), the s_{ij}^P are the elastic compliance coefficients at constant polarization, and the Q_{ij} have been defined in equation (4). Techniques for determining the α_1^σ, α_i^σ, α_{ijk}^σ, and Q_{ij} (as well as their temperature dependence) have been described and discussed extensively in, for example, references [26–28]: the dielectric stiffness α_1^σ which depends linearly on temperature can be obtain from the Curie–Weiss law, the α_{ij}^σ and σ_{ijk}^σ are usually determined by correlating them with the spontaneous polarization measured at the Curie point, and the Q_{ij} may be solved from the relations between the lattice deformation and the polarization (see equation (3)). Provided that these coefficients are given, determination of the expansion coefficients in equation (2) is as follows.

Since the original cubic structure of perovskites is centro-symmetric, one has $\alpha_1 = \alpha_1^\sigma$. For the stress-free state (i.e. $\sigma_{ij} = 0$), G and F are identical, which indicates from equations (2), (5) and (57) that $\alpha'_{ij} = \alpha_{ij}^\sigma$ and $\alpha_{ijk} = \alpha_{ijk}^\sigma$. Furthermore, because Q_{ij} and the second-order elastic constants c_{ij} (or the elastic compliance coefficients s_{ij}^P) can be measured directly, the electrostrictive coefficients q_{ij} are obtainable from equation (4). As the c_{ij}, q_{ij}, and α'_{ij} are known, one may obtain α_{ij} from equation (5). Finally, Cao [29] has correlated the polarization gradient coefficients g_{ij} in equation (8) with the dispersion surface of the soft mode of perovskites, and on the basis of this correlation, the three gradient coefficients can, in principle, be determined through measurements along the three principal directions in inelastic neutron scattering experiments.

In most cases, all of the coefficients in equations (2) and (8) except α_1 are weakly temperature dependent. Therefore, for a semi-quantitative description of the walls, these macroscopic quantities are measured near the Curie point and assumed constant in all of the ferroelectric phases. In this manner, the results show that the increase of α_1 upon heating can lead to an increase of the wall width and a decrease of the wall energy, which is a common feature for ferroic domain walls and has been verified by experiments [17, 18, 30]. For a more accurate quantification, the variation of the higher-order coefficients with temperature must be considered. Fortunately, by correlating the dielectric, piezoelectric, and elastic properties of the perovskites, these parameters in the orthorhombic phase can be extrapolated from the values obtained near the Curie point [27, 28]. When the temperature dependence of all of the coefficients is known, one can deduce the exact profiles of the polarization, strains, and clamping stresses for a domain wall at any temperature point. At present, the experimental results concerning the domain wall structures in orthorhombic perovskites are

sparse, but some direct measurements performed on the walls in the tetragonal phase may prove the validity of the present theory. For example, Zhang, Hashimoto, and Joy [31] have studied the 90° walls in tetragonal $BaTiO_3$ using electron holography. Comparing figure 3 of reference [31] and figure 2 of the present paper, one can find that the polarization profile obtained experimentally is, indeed, very similar to the kink solutions of equations (25), (36), and (53) instead of the equation $P_z = P_0 \tanh(x/\delta)$ which is for second-order phase transitions. (Note that the Ising-type walls in the tetragonal phase also have kink solutions according to the present theory.)

It should be noted that in a uniaxial ferroelectric crystal, the (180°) domain walls are always of Ising type. However, since the spontaneous polarization of ferroelectric perovskites can take more than one components along the three ⟨100⟩ axes of the cubic structure, the domain walls may appear in either Ising-type or Bloch-type configurations. In fact, the possible existence of the Bloch-type domain wall is a unique property of perovskite crystals. For such a interfacial structure, the polarization component along the direction parallel to the wall spirals from the original direction to the opposite direction across the wall layer. Generally, the wall structure with relatively lower energy is thermodynamically stable. The existence of Bloch-type walls in perovskites may be proved by the fact that the 180° walls in $BaTiO_3$ are directly visible between crossed polarizers even with no external electric field normal to the polar axis applied [32]. Since the Ising-type 180° walls are invisible from considerations of lattice symmetry, the 180° walls observable under polarized light are believed to be of Bloch type [25].

The most complicated domain wall in orthorhombic perovskites is the 60° wall whose orientation cannot be described by a crystallographic plane (the W′ wall) [13]. This kind of wall occurs only within the high-temperature range or in significantly inhomogeneous crystals. But, by the same procedure as presented in this paper, one can obtain similar results for the detailed wall structure in a suitably transformed coordinate system. In this sense, the above treatment for 180°, 90°, and 120° walls provides a general ϕ^6-model for predicting domain wall structures in real perovskites associated with the first-order ferroelectric phase transitions, and it can be extended to describe any kinds of twin structure in all of the three ferroelectric phases.

Acknowledgments

This work was supported by the National Natural Science Foundation of China and National Laboratory of BEPC, Institute of High Energy Physics, People's Republic of China.

References

[1] Jona F and Shirane G 1962 *Ferroelectric Crystals* (Oxford: Pergamon)
[2] Triebwasser S 1959 *Phys. Rev.* **114** 63
[3] Huang X R, Jiang S S, Xu X Y, Wang J Y, Guan Q C, Jiang J H and Feng D 1995 *Phys. Status Solidi* a **148** 611
[4] Deshmukh K G and Ingle S G 1971 *J. Phys. D: Appl. Phys.* **4** 124
[5] Merz W J 1954 *Phys. Rev.* **95** 690
[6] Little E A 1955 *Phys. Rev.* **98** 978
[7] Tsai F and Cowley J M 1993 *Ferroelectrics* **140** 203
[8] Nambu S and Sagala D A 1994 *Phys. Rev.* B **50** 5838
[9] Wiesendanger E 1973 *Czech. J. Phys.* B **23** 91
[10] Janovec V 1976 *Ferroelectrics* **12** 43
[11] Dudnik E F and Shuvalov L A 1988 *Ferroelectrics* **98** 207

[12] Huang X R, Jiang S S, Liu W J, Wu X S, Feng D, Wang Z G, Han Y and Wang J Y 1996 *J. Appl. Crystallogr.* **29** 371
[13] Boulesteix C 1984 *Phys. Status Solidi* a **86** 11
[14] Lines M E and Glass A M 1977 *Principles and Applications of Ferroelectrics and Related Materials* (Oxford: Clarendon)
[15] Salje E K H 1991 *Phase Transitions* **34** 25
[16] Cao W and Cross L E 1991 *Phys. Rev.* B **44** 5
[17] Andrews S R and Cowley R A 1986 *J. Phys. C: Solid State Phys.* **19** 615
[18] Huang X R, Jiang S S, Hu X B, Xu X Y, Zeng W, Feng D and Wang J Y 1995 *Phys. Rev.* B **52** 9932
[19] Cao W and Randall C 1993 *Solid State Commun.* **86** 435
[20] Chen J, Wang W S, Li Q and Feng D 1988 *Cryst. Res. Technol.* **23** 747
[21] Mitsui T, Mitsuzaki T and Nakamura E 1976 *An Introduction to the Physics of Ferroelectrics* (New York: Gordon and Breach) p 142
[22] Barber J R 1992 *Elasticity* (Dordrecht: Kluwer Academic) p 22
[23] Gordon A 1983 *Physica* B **122** 321
[24] Lajzerowicz J and Houchmandzadeh B 1993 *Ferroelectrics* **140** 81
[25] Huang X R, Hu X B, Jiang S S and Feng D 1997 *Phys. Rev.* B **55** 5534
[26] Drougard M E and Huibregtse E J 1957 *IBM. J. Res. Dev.* **1** 318
[27] Amin A, Haun M J, Badger B, McKinstry H and Cross L E 1985 *Ferroelectrics* **65** 107
[28] Haun M J, Furman E, Jang S J, McKinstry H A and Cross L E 1987 *J. Appl. Phys.* **62** 3331
[29] Cao W 1994 *J. Phys. Soc. Japan* **63** 1156
[30] Robert M, Reaney I and Stadelmann P 1996 *Physica* A **229** 47
[31] Zhang X, Hashimoto T and Joy D C 1992 *Appl. Phys. Lett.* **60** 784
[32] Kobayashi J and Yamada N 1963 *Phys. Rev. Lett.* **11** 410